Fano Resonant Ring/Disk Plasmonic Nanocavities on Conducting Substrates for Advanced Biosensing

Arif E. Cetin and Hatice Altug*

Department of Electrical and Computer Engineering, Boston University, Boston, Massachusetts 02215, United States

ABSTRACT By introducing a conducting metal layer underneath a Fano resonant asymmetric ring/disk plasmonic nanocavity system, we demonstrate that electromagnetic fields can be strongly enhanced. These large electromagnetic fields extending deep into the medium are highly accessible and increase the interaction volume of analytes and optical fields. As a result, we demonstrate high refractive index sensitivities as large as 648 nm/RIU. By exciting Fano resonances with much sharper spectral features, as narrow as 9 nm, we experimentally show high figure of merits as large as 72 and reliable detection of protein mono- and bilayers. Furthermore, the conducting substrate enables strong interaction between fundamental and higher order modes of the system by minor structural asymmetries. This is very advantageous for experimental realization of systems supporting resonances with well-defined Fano-like line shape without requiring challenging fabrication resolution. Exploiting conducting metallic substrates and the associated propagating surface plasmons at their interface could be extended to other Fano resonant cavity geometries for improved biosensing performance.

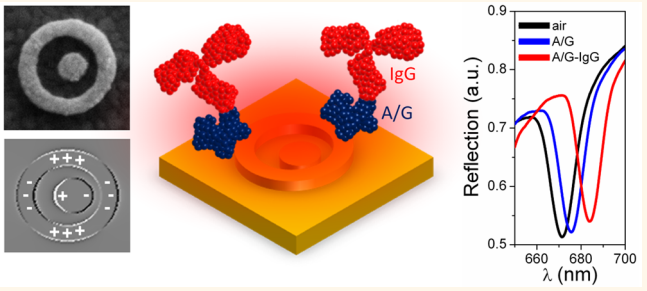

KEYWORDS: plasmonics · Fano interference · ultrasensitive biosensing · figure of merit · refractive index sensitivity · nanocavities · nanofabrication

Science and engineering of surface plasmons concentrated at a metal/dielectric interface has opened up a wide range of applications from biosensing and surface-enhanced spectroscopy to optical trapping.[1−15] Most of these applications greatly benefit from unique properties of metallic structures that enable strong light/matter interactions.[16−20] The local electromagnetic fields supported by metallic features are highly enhanced at a resonance frequency of a dipolar plasmonic mode which depends on the geometry and size of the nanostructures.[21,22] Recently, many groups have presented different designs to access this fundamental mode such as ring[23−26] or disk[27,28] nanocavities. Although these metallic structures support high near-field enhancements at this dipolar resonance, its line width determined by the radiative and nonradiative losses is relatively broad. Nonradiative losses mainly depend on the properties of metal composing the nanostructure. Radiative losses, in contrast, can be controlled through the hybridization of plasmons enabled by coupling between closely positioned nanostructures.[29] Accordingly, Hao *et al.* proposed a ring/disk cavity system which reduces the radiative losses by bringing ring and disk structures in close proximity.[30] The proposed concentric system composed of a disk embedded in the center of a ring has been shown to exhibit sub- and super-radiant modes *via* hybridization between dipolar modes of ring and disk cavities. Interestingly, by introducing structural symmetry-breaking to the system, they demonstrated Fano-type resonances excited due to the coupling between the dipolar mode of the disk and the higher order mode of the ring cavity.[21] Later, Sonnefraud *et al.* demonstrated the possibility of using asymmetric ring/disk cavities in biochemical sensing applications.[31] Biochemical sensing platforms exhibit high sensitivities to surface conditions when the field profiles enable strong interaction with the surrounding medium. The asymmetric ring/disk cavity systems fabricated on a dielectric substrate

* Address correspondence to altug@bu.edu.

Received for review August 11, 2012 and accepted October 23, 2012.

Published online October 23, 2012
10.1021/nn303643w

offer narrower resonances; however, the enhancement in their local electromagnetic fields is relatively low. More importantly, these local fields are highly inaccessible to the surrounding medium since they are mainly concentrated at the high refractive index substrate under the nanocavities. Furthermore, biochemical sensing platforms demand narrow resonances to accurately measure variations in cavity response due to the presence of the molecules. Even though Fano resonances supported by an asymmetric nanocavity system fabricated on a dielectric layer exhibit narrower resonances compared to dipolar modes, they are still relatively broad for achieving low limit of detection.[32] Therefore, new approaches to exploit Fano resonances are needed to address these limitations.

In this article, we experimentally demonstrate a Fano resonant asymmetric ring/disk system fabricated on a conducting substrate which possesses superior far- and near-field characteristics compared to the one fabricated on a dielectric substrate. The proposed platform is shown to exhibit much higher near-field intensity enhancements. More importantly, these large local fields supported by the system extend deep into the surrounding medium, which makes them easily accessible to biochemical molecules in the vicinity. Hence, the platform by strongly increasing the interaction volume of the analytes and the local fields offers larger sensitivities to changes in surface conditions. We experimentally demonstrate that asymmetric ring/disk cavities fabricated on a conducting metal layer provide refractive index sensitivities as large as 648 nm/RIU (refractive index unit). The proposed cavity system is shown to support Fano-type resonances that can exhibit spectrally sharp features with line widths as narrow as 9 nm due to the contribution of sub- and super-radiant modes as well as propagating surface plasmons residing at the surface of the conducting substrate. Consequently, we demonstrate that the platform provides experimentally measured figure of merits as large as 72 and enables reliable detection of protein mono/bilayers. We also show that the system standing on a conducting substrate supports stronger Fano resonances with sharper spectral features through minor structural asymmetries. This is highly advantageous as we do not need extremely small gaps between constituting ring and disk elements demanding strict fabrication resolution.

RESULTS AND DISCUSSION

Figure 1a schematically shows the asymmetric ring/disk system standing on a conducting metal layer, and Figure 1b is the scanning electron microscope image of the fabricated structures that are experimentally tested. Here, the radius of the disk (R_{disk}), inner radius (R_{inner}), and outer radius of the ring (R_{outer}) are 90, 160, and 240 nm, respectively. For our platform, the amount

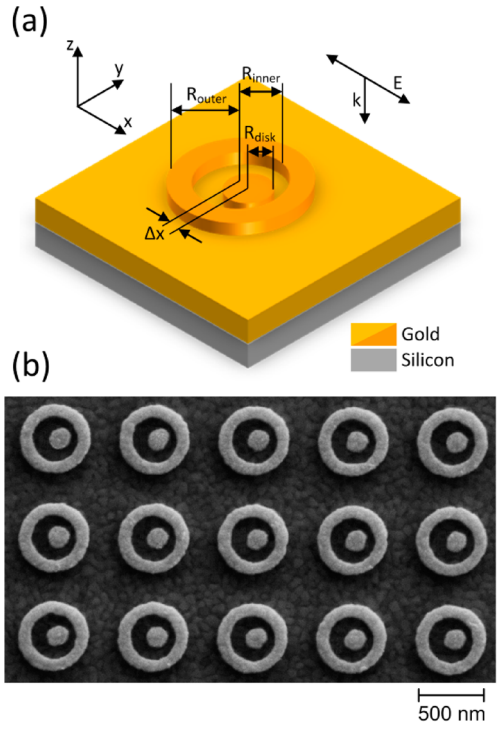

Figure 1. (a) Schematic view of the asymmetric ring/disk system fabricated on a conducting layer. Geometrical parameters of the structure, propagation direction, and polarization of the illumination source are indicated in the figure. (b) Scanning electron microscope image of the fabricated asymmetric ring/disk cavity on a conducting layer. Corresponding structure parameters are R_{disk} = 90 nm, R_{inner} = 160 nm, R_{outer} = 240 nm, and Δx = 30 nm. Periodicity of the cavity array is 750 nm, and thickness of the asymmetric ring/disk cavity and the gold conducting metal layer is 100 and 150 nm, respectively.

of the structural symmetry-breaking is determined by Δx, which is the shifting amount of the disk from the center of the concentric system along the polarization direction. For the structure presented in the figure, Δx is 30 nm. The thickness of the ring and disk cavities is 100 nm, and the period of the ring/disk cavity array is 750 nm.

Concentric ring/disk systems fabricated on a conducting gold layer exhibit sub- and super-radiant characteristics *via* hybridization between the dipolar modes of the ring and disk cavities (see Supporting Information for detail). By introducing structural asymmetries, these systems can excite Fano-type resonances exhibiting spectrally sharp features of narrow line width, as shown in Figure 2a.[31] Fano resonance occurs in the presence of interference between a spectrally broad and a narrow mode.[33,34] Phase-lag and the relative amplitude difference between these two modes lead to a highly dispersive Fano resonance with a very asymmetric spectral profile.[33] In our system, Fano-type asymmetric resonance is created through the overlap between the super-radiant hybridized dipolar mode which is a bonding combination of dipolar disk and antibonding ring modes (DAR mode), acting as the

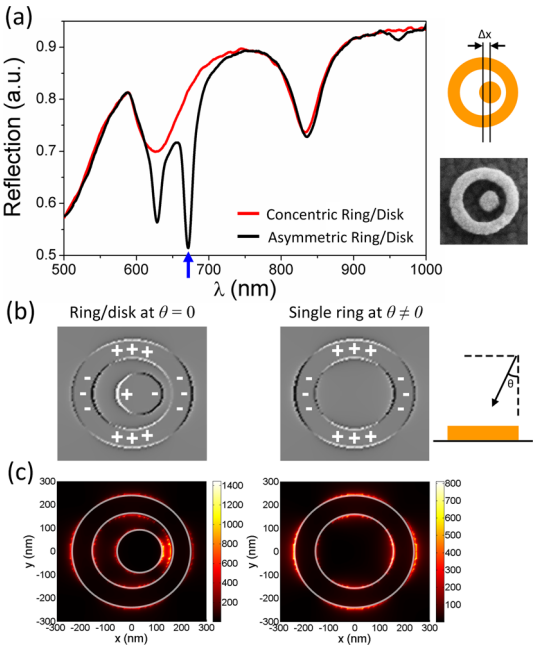

Figure 2. (a) Experimental reflection spectrum of concentric (red curve) and asymmetric ring/disk cavities fabricated on a conducting layer with Δx = 30 nm (black curve). On the right, schematic illustration of the shifting procedure of the disk element and the scanning electron microscope image of the fabricated asymmetric ring/disk cavity with Δx = 30 nm on a conducting metal layer are shown. (b) Charge and (c) electric field intensity enhancement distributions of the asymmetric ring/disk cavity system under normal incidence (left) and the ring cavity at an incident angle θ (right) calculated at the top surface. The periodicity of the structures is kept at 750 nm.

bright state of the composite system, and the narrow quadrupolar ring mode,[19,21] acting as the dark state. Compared to the conventional dielectric system, here we also have an additional contribution from surface plasmon polaritons at the conducting metal/dielectric interface (see Supporting Information for detail). The interaction of surface plasmon polaritons with the hybridized modes of the ring/disk cavity could modify the spectrum and results in sharper spectral features within the Fano resonance. For an asymmetric ring/disk cavity system with 30 nm offset, we experimentally observe excitation of a Fano-type resonance exhibiting two narrow spectral features. For our analyses, we focus on the sharper one at 672 nm (indicated by a blue arrow in Figure 2a). It has a narrow line width as small as 9 nm. For a ring cavity under normal incidence (nonretarded case), the quadrupolar mode cannot be excited due to the symmetric charge distribution which makes the total dipole moment zero. When an incident angle is introduced, the quadrupolar mode is excited through the retardation effects.[35] Figure 2b (right) is the charge distribution (calculated at 672 nm) of the ring cavity under an incident angle (θ) demonstrating the quadrupolar characteristics. Since the quadrupolar modes cannot be directly coupled to the far-field radiation, their radiative losses are very small, which leads to spectrally sharp features. For the strongly coupled asymmetric ring/disk cavity, quadrupolar mode appears at the Fano resonance, as indicated by the charge distribution calculated at 672 nm (Figure 2b, left).[36,37] At this wavelength, under normal incidence (Figure 2c, left), the asymmetric ring/disk cavity system exhibits similar field profile at the constituting ring element with the one supported by the ring cavity under an incident angle, θ (Figure 2c, right). This quadrupolar nature can be observed at different wavelengths of the Fano resonance (see Supporting Information for detail).

One advantage of using the asymmetric ring/disk cavity platform fabricated on a conducting metal layer is the desirable near-field characteristics for biosensing applications. The cavity system standing on a conducting substrate enables much higher near-field intensity enhancements compared to the identical one standing on a dielectric substrate. More importantly, these large local electromagnetic fields are easily accessible to the surrounding medium. In order to show this, we compare near-field profiles on both substrates at their corresponding sharp spectral features indicated by red arrows (reflection dip at 672 nm and reflection peak at 967 nm for the cavity on conducting (Figure 3a) and dielectric (Figure 3b) layers, respectively). We observe that asymmetric ring/disk cavities on a conducting metal layer studied in this work supports a nearly 4 times higher near-field intensity enhancement. The field intensity enhancement varies with wavelength within the Fano-like asymmetric line shape.[38] We observe that the system on a conducting layer has much higher near-field intensity enhancement compared to its counterpart on dielectric at all wavelengths within the Fano resonance (see Supporting Information for detail). In addition, when there is a conducting layer underneath the cavities, the cross-sectional field profiles show that highly enhanced near-fields are mainly concentrated at the top surface of the ring/disk cavities and extend deep into the surrounding medium. This is in sharp contrast for the one on a glass layer where most of the enhanced local fields are mainly concentrated at the metal/glass interface and not directly accessible. We observe that similar improvements in near-field characteristics achieved by introducing a conducting metal layer underneath could be extended to other plasmonic Fano resonant structures such as dolmen-shaped cavities (see Supporting Information for detail).

In order to quantitatively demonstrate the field accessibility, we calculate a volume in the vicinity of the cavity array by considering the regions where the maximum field intensity drops by a factor of $1/e^2$. We term this volume as the "interaction volume" of analyte and optical fields. For both asymmetric ring/disk cavity systems studied in this work, we calculate near-field intensity enhancement ($|E|^2/|E_{in}|^2$) distributions and

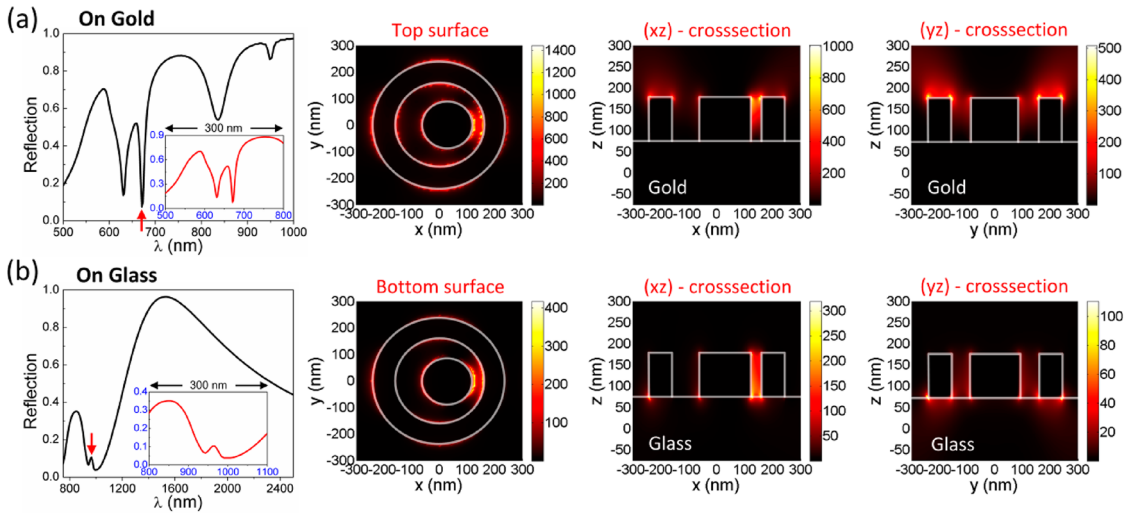

Figure 3. Calculated reflection spectrum and near-field intensity enhancement distributions at the sharp spectral feature (centered at 672 nm for the cavity array on a conducting layer and at 967 nm for the cavity array on a dielectric layer) within the Fano-type resonance for the asymmetric ring/disk cavity system with Δx = 30 nm on (a) conducting and (b) dielectric layers at different cross sections. The *xy* near-field distributions are calculated at the top surface of the cavity on a gold layer and at the bottom surface of the cavity on a glass layer. The *xz* (*yz*) cross-sectional field profiles are calculated through the center of the system, $y = 0$ ($x = 0$). For clarification of the spectral comparison, the spectral ranges of two figures are zoomed within a 300 nm wavelength window in the insets.

determine their maximum. Since the maximum intensity for the system on glass (I_{glass} = 400) is significantly smaller than the one for gold (I_{gold} = 1400), we set $1/e^2$ of I_{glass} as the cutoff intensity. We then determine the volume where the field intensity drops to this cutoff value. In Table 1, we compare the interaction volumes at the spectral features denoted by the red arrows in Figure 3. Asymmetric ring/disk cavity system on a conducting metal layer is observed to support nearly 4 times larger interaction volume compared to the one on a dielectric layer. In addition, we numerically calculate the refractive index sensitivity, which is defined as the change in the resonance wavelength with respect to the change in the refractive index of the bulk solution ($S = \Delta\lambda/\Delta n$). Between the two systems embedded in DI water, the one standing on a conducting metal layer supports a higher refractive index sensitivity compared to the one standing on a dielectric layer, 667 *vs* 545 nm/RIU, respectively. Another advantage of using a conducting metallic substrate is the excitation of sharp spectral features which can significantly reduce the limit of detection. As demonstrated in the table, the system on a conducting layer supports a spectral feature more than 3 times narrower. Exhibiting much sharper spectral features as well as larger refractive index sensitivities, the asymmetric ring/disk system on a conducting layer supports nearly a 4 times larger figure of merit (FOM = *S*/FWHM where FWHM is full width at half maximum). In this work, we use gold as the conducting metallic substrate. Similar improvements in near- and far-field responses are also observed for different metallic substrates including silver.

Supporting easily accessible large field intensities as well as spectrally sharp features, our asymmetric ring/disk cavity system is a good candidate for ultrasensitive biodetection. We experimentally demonstrate its sensing capability by monitoring the variations in the sharp spectral feature within the Fano resonance after introducing bulk solutions with different refractive indices, including deionized water n_{DI} = 1.333, acetone $n_{acetone}$ = 1.356, and IPA n_{IPA} = 1.377, as shown in Figure 4a. The cavity system on a conducting layer is shown to exhibit an experimental refractive index sensitivity as large 648 nm/RIU. With spectral line width as small as 9 nm, we experimentally obtain a large figure of merit, 72. We also perform a label-free sensing of protein monolayer and bilayer with the asymmetric ring/disk cavity platform by measuring the reflection spectrum and monitoring the variations after addition of protein layers (see Methods section for protein chemistry and preparation), as shown in Figure 4b.[39,40] To form a protein monolayer, we utilize protein A/G which is a recombinant fusion protein constituting binding domains of both protein A and protein G. Protein A/G sticks on the gold surface by physisorption.[7,8,39] Due to the accumulated biomass on the sensor surface, which increases the local refractive index, attachment of 1 mg/mL

TABLE 1. Comparison of the Interaction Volume, Full Width at Half-Maximum (FWHM), Refractive Index Sensitivity (*S*), and Figure of Merit (FOM) between Asymmetric Ring/Disk Cavity Systems Standing on Conducting and Dielectric Layers for the Spectral Features Indicated by Red Arrows in Figure 3a,b

	interaction volume (nm^3)	FWHM (nm)	*S* (nm/RIU)	FOM
cavity on gold	50.2×10^6	9	667	75
cavity on glass	12.7×10^6	28	545	20

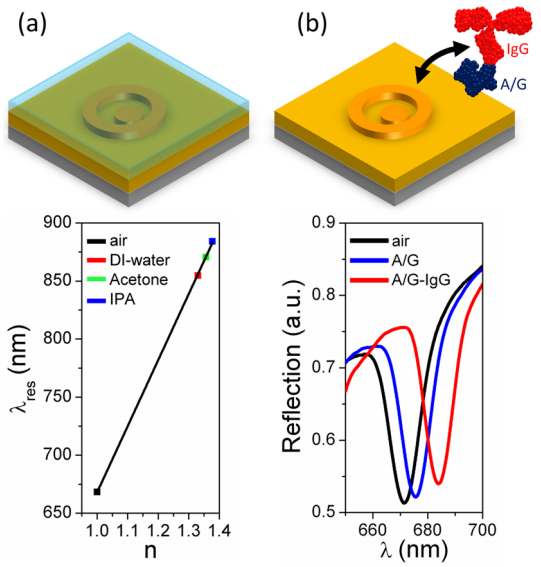

Figure 4. Variations in the spectral feature centered at 672 nm after introducing (a) bulk solutions with different refractive indices, DI water n_{DI} = 1.333, acetone $n_{acetone}$ = 1.356, and IPA n_{IPA} = 1.377, and (b) 1 mg/mL protein A/G and 1 mg/mL IgG antibody.

A/G results in a 5 nm red shift in the spectral feature within the Fano resonance. To form the protein bilayer, antibody IgG is immobilized on protein A/G due to the high affinity of protein A/G to the Fc regions of antibody IgG.[7,8,39] We can reliably detect that 1 mg/mL IgG results in a total of 14 nm red shift in the spectral feature.

Fano resonance highly depends on the coupling between dipolar and quadrupolar antennas. This coupling, proportional to Δx, successively increases with structural asymmetry. Therefore, we investigate the appearance of Fano resonance and its dependence on Δx for both systems. Figure 5a,b shows the calculated reflection spectra with Δx values ranging from 0 to 40 nm. For identical dimensions, the system on a conducting metal layer supports a sharp spectral feature denoted by a blue arrow within the spectral window of 650−700 nm, whereas for the one on a dielectric layer, the spectral feature shifts to longer wavelengths, 900−1000 nm. With increasing Δx, the feature gets increasingly stronger for both systems. More importantly, the ring/disk system on a conducting layer can excite sharp spectral features with minor structural asymmetry, as small as 10 nm, while a much larger asymmetry, 30 nm, is necessary for the other system. The spectral strength of the Fano resonance (the contrast between the reflection maximum/minimum with the baseline) obtained with Δx = 40 nm using the ring/disk cavity system on a dielectric layer can be achieved with only $\Delta x \approx$ 15 nm by the system on a conducting layer. The ring/disk cavity systems on conducting and dielectric layers with identical geometry excite Fano resonances in different wavelength ranges. In order for these two systems to have a Fano resonance in a similar spectral window, they require very different device dimensions. For example, to be within 650−700 nm range, the ring/disk system on a conducting metal layer has device dimensions: R_{disk} = 90 nm, R_{inner} = 160 nm, and R_{outer} = 240 nm. However, the system on a dielectric layer needs much smaller dimensions: R_{disk} = 33 nm, R_{inner} = 45 nm, and R_{outer} = 70 nm. Furthermore, since the sharp spectral feature is excited through smaller structural asymmetry for the ring/disk system on a conducting layer, relatively larger gap between the constituting disk and ring elements, 40 nm, is necessary. In contrast, to achieve a strong coupling between dipolar and quadrupolar modes, the system on a dielectric layer needs a gap as small as 6 nm. Hence, the ring/disk cavity system on a dielectric layer demands more challenging fabrication requirements. Appearance of the sharper spectral feature through smaller structural asymmetries on a gold surface indicates that the presence of the conducting layer enables much stronger coupling between the dipolar and quadrupolar modes. This is partly facilitated by the contribution of propagating surface plasmons on the conducting layer and air interface excited by the grating effect.

CONCLUSION

In conclusion, by introducing a conducting metal layer underneath the closely placed plasmonic nanostructures, we demonstrate that stronger near-field enhancements can be achieved. In comparison to the nanostructures on a dielectric, our approach can access low-loss quadrupolar modes more efficiently and results in Fano resonances with much sharper spectral features. These large electromagnetic fields supported by the strongly coupled nanostructures extend deep into the surrounding medium and greatly enhance the accessibility of the optical fields. Field profiles allowing large interaction volumes between analytes and optical fields are important for many applications, particularly biosensing. We demonstrate that our system based on coupled asymmetric ring/disk cavities enables reliable detection of protein mono- and bilayers. Furthermore, conducting metallic substrates by enabling stronger interaction between fundamental and higher order modes of the nanostructures as well as propagating surface plasmons at the conducting interface can lead to Fano resonances with only minor structural asymmetries, thus helping to reduce fabrication tolerance.

METHODS

FDTD Simulations. Far- and near-field responses of ring/disk cavities are analyzed through three-dimensional finite-difference time-domain (3D-FDTD) simulations. In simulations, the dielectric constant of silicon, glass, and gold is taken from ref 41. For the unit cell consisting of a ring/disk cavity, periodic boundary condition is used along the *x*- and *y*-directions, and perfectly matched layer boundary condition is used along the direction of the illumination source, *z*. In the simulations, the mesh size

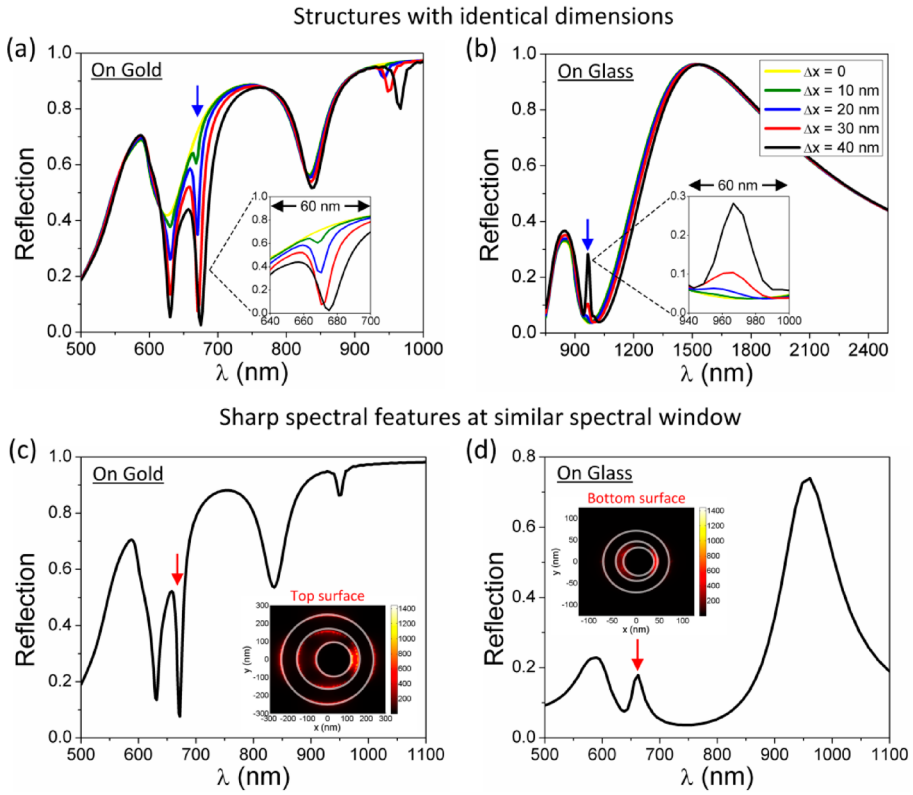

Figure 5. Dependence of the sharp spectral feature denoted by a blue arrow on the offset from the center of the concentric system, Δx for asymmetric ring/disk cavity on (a) conducting and (b) dielectric layers with identical dimensions. For clarification of the spectral comparison, the analyzed spectral features are zoomed within a 60 nm wavelength window in the insets. Calculated reflection spectrum of the asymmetric ring/disk cavity on (c) conducting and (d) dielectric layers supporting features in the same spectral window. In the insets, near-field intensity enhancement distributions are calculated at the sharp spectral features denoted by red arrows for the system on conducting (at the top surface of the cavity, at 672 nm) and dielectric layers (at the bottom surface of the cavity, at 688 nm).

is chosen to be 5 nm along the *x*-, *y*-, and *z*-directions. The numerical calculations are performed with extremely well convergence conditions with different mesh sizes down to 2 nm, and similar near- and far-field responses are obtained.

Protein Chemistry and Preparation. For protein immobilization, we perform the following steps. First, ring/disk cavities are cleaned by a piranha solution (H_2SO_4/H_2O_2 = 3:1) and rinsed with DI water to dissipate any organic contamination on the surface. To form the protein monolayer, 1 mg/mL A/G is spotted on the chip surface and incubated for 1 h. We then rinse the chip with PBS (phosphate buffer) to remove the unbound protein. To form the protein bilayer, 1 mg/mL IgG is spotted on the chip surface and incubated for another 1 h. Finally, a second washing process is performed to remove the unbound protein.

Spectral Measurements. All spectral measurements are performed by a Nikon Eclipse-Ti microscope coupled to a SpectraPro 500i spectrometer. A normally incident light is used to illuminate the chip. Reflected data are then normalized using a thick gold standard.

Fabrication of Ring/Disk Cavities on a Conducting Layer. Fabrication starts by depositing 150 nm thick gold on a silicon wafer using a directional electron-beam evaporator. We then perform electron-beam lithography (EBL) using a positive resist, polymethyl methacrylate (PMMA). The EBL-defined patterns are developed by a methyl isobutyl ketone/isopropyl alcohol (MIBK-IPA) solution. Next, 100 nm thick gold is deposited followed with a lift-off process. As a final step, a plasma cleaning process (O_2 cleaning) is performed to remove any leftover EBL resist.

Conflict of Interest: The authors declare no competing financial interest.

Acknowledgment. This research was supported by the National Science Foundation (NSF) CAREER Award ECCS-0954790, ONR Young Investigator Award 11PR00755-00-P00001, and NSF Engineering Research Center on Smart Lighting EEC-0812056.

Supporting Information Available: (i) Contribution of propagating surface plasmons for excitation of sharper spectral features within the Fano resonance. (ii) Numerical comparison of far- and near-field responses of Fano resonant dolmen structures on dielectric and conducting layers. (iii) Theoretical and experimental analyses of concentric ring/disk cavity systems. (iv) Charge and near-field intensity enhancement distributions of asymmetric ring/disk cavity systems on conducting and dielectric layers within Fano resonance. This material is available free of charge *via* the Internet at http://pubs.acs.org.

REFERENCES AND NOTES

1. Lal, S.; Link, S.; Halas, N. J. Nano-Optics from Sensing to Waveguiding. *Nat. Photonics* **2007**, *1*, 641–648.
2. Atwater, H. A.; Polman, A. Plasmonics for Improved Photovoltaic Devices. *Nat. Mater.* **2010**, *9*, 205–212.
3. Lukyanchuk, B.; Zheludev, N. I.; Maier, S. A.; Halas, N. J.; Nordlander, P.; Giessen, H.; Chong, C. T. The Fano Resonance in Plasmonic Nanostructures and Metamaterials. *Nat. Mater.* **2010**, *9*, 707–715.
4. Juan, M. L.; Righini, M.; Quidant, R. Plasmon Nano-Optical Tweezers. *Nat. Photonics* **2011**, *5*, 349–356.
5. Kneipp, K.; Wang, Y.; Kneipp, H.; Perelman, L. T.; Itzkan, I.; Dasari, R. R.; Feld, M. S. Single Molecule Detection Using Surface-Enhanced Raman Scattering (SERS). *Phys. Rev. Lett.* **1997**, *78*, 1667–1670.
6. Kundu, J.; Le, F.; Nordlander, P.; Halas, N. J. Surface Enhanced Infrared Absorption (SEIRA) Spectroscopy on Nanoshell Aggregate Substrates. *Chem. Phys. Lett.* **2008**, *452*, 115–119.

7. Adato, R.; Yanik, A. A.; Amsden, J. J.; Kaplan, D. L.; Omenetto, F. G.; Hong, M. K.; Erramilli, S.; Altug, H. Ultra-Sensitive Vibrational Spectroscopy of Protein Monolayers with Plasmonic Nanoantenna Arrays. *Proc. Natl. Acad. Sci. U.S.A.* **2009**, *106*, 19227–19232.
8. Yanik, A. A.; Cetin, A. E.; Huang, M.; Artar, A.; Mousavi, S. H.; Khanikaev, A.; Connor, J. H.; Shvets, G.; Altug, H. Seeing Protein Monolayers with Naked Eye through Plasmonic Fano Resonances. *Proc. Natl. Acad. Sci. U.S.A.* **2011**, *108*, 11784–11789.
9. Kim, S.; Jin, J.; Kim, Y. J.; Park, I. Y.; Kim, Y.; Kim, S. W. High-Harmonic Generation by Resonant Plasmon Field Enhancement. *Nature* **2008**, *453*, 757–760.
10. Kinkhabwala, A.; Yu, Z.; Fan, S.; Avlasevich, Y.; Mullen, K.; Moerner, W. E. Large Single-Molecule Fluorescence Enhancements Produced by a Bowtie Nanoantenna. *Nat. Photonics* **2009**, *3*, 654–657.
11. Sorger, V. J.; Pholchai, N.; Cubukcu, E.; Oulton, R. F.; Kolchin, P.; Borschel, C.; Gnauck, M.; Ronning, C.; Zhang, X. Large Strongly Enhanced Molecular Fluorescence inside a Nanoscale Waveguide Gap. *Nano Lett.* **2011**, *11*, 4907–4911.
12. Zia, R.; Brongersma, M. L. Surface Plasmon-Polariton Analogue to Young's Double Slit Experiment. *Nat. Nanotechnol.* **2007**, *2*, 426–429.
13. Aydin, K.; Ferry, V. E.; Briggs, R. M.; Atwater, H. A. Broadband, Polarization-Independent Resonant Light Absorption Using Ultrathin, Plasmonic Super Absorbers. *Nat. Commun.* **2011**, *2*, 517.
14. Bulu, I.; Babinec, T.; Hausmann, B.; Choy, J. T.; Loncar, M. Plasmonic Resonators for Enhanced Diamond NV-Center Single Photon Sources. *Opt. Express* **2011**, *19*, 5268–5276.
15. Cetin, A. E.; Yanik, A. A.; Yilmaz, C.; Somu, S.; Busnaina, A. A.; Altug, H. Monopole Antenna Arrays for Optical Trapping, Spectroscopy and Sensing. *Appl. Phys. Lett.* **2011**, *98*, 111110.
16. Maier, S. A.; Atwater, H. A. Plasmonics: Localization and Guiding of Electromagnetic Energy in Metal/Dielectric Structures. *J. Appl. Phys.* **2005**, *98*, 011101.
17. Zhou, W.; Odom, T. W. Tunable Subradiant Lattice Plasmons by Out-of-Plane Dipolar Interactions. *Nat. Nanotechnol.* **2011**, *6*, 423–427.
18. Liberman, V.; Yilmaz, C.; Bloomstein, T. M.; Somu, S.; Echegoyen, Y.; Busnaina, A.; Cann, S. G.; Krohn, K. E.; Marchant, M. F.; Rothschild, M. A Nanoparticle Convective Directed Assembly Process for the Fabrication of Periodic Surface Enhanced Raman Spectroscopy Substrates. *Adv. Mater.* **2010**, *22*, 4298–4302.
19. Nordlander, P.; Oubre, C.; Prodan, E.; Li, K.; Stockman, I. Plasmon Hybridization in Nanoparticle Dimers. *Nano Lett.* **2004**, *4*, 899–903.
20. Pryce, I. M.; Kelaita, Y. A.; Aydin, K.; Briggs, R. M.; Atwater, H. A. Compliant Metamaterials for Resonantly Enhanced Infrared Absorption Spectroscopy and Refractive Index Sensing. *ACS Nano* **2011**, *5*, 8167–8174.
21. Hao, F.; Nordlander, P.; Sonnefraud, Y.; Dorpe, P. V.; Maier, S. A. Tunability of Subradiant Dipolar and Fano-Type Plasmon Resonances in Metallic Ring/Disk Cavities: Implications for Nanoscale Optical Sensing. *ACS Nano* **2009**, *3*, 643–652.
22. Hao, F.; Sonnefraud, Y.; Dorpe, P. V.; Maier, S. A.; Halas, N. J.; Nordlander, P. Symmetry Breaking in Plasmonic Nanocavities: Subradiant LSPR Sensing and a Tunable Fano Resonance. *Nano Lett.* **2008**, *8*, 3983–3988.
23. Link, S.; El-Sayed, M. A. Shape and Size Dependence of Radiative, Non-radiative and Photothermal Properties of Gold Nanocrystals. *Int. Rev. Phys. Chem.* **2000**, *19*, 409–453.
24. Aizpurua, J.; Hanarp, P.; Sutherland, D. S.; Kall, M.; Bryant, G. W.; Garcia de Abajo, F. J. Optical Properties of Gold Nanorings. *Phys. Rev. Lett.* **2003**, *90*, 057401.
25. Kim, S.; Jun, J. M.; Choi, D. G.; Jung, H. T.; Yang, S. M. Patterned Arrays of Au rings for Localized Surface Plasmon Resonance. *Langmuir* **2006**, *22*, 7109–7112.
26. Larsson, E. M.; Alegret, J.; Kall, M.; Sutherland, D. S. Sensing Characteristics of NIR Localized Surface Plasmon Resonances in Gold Nanorings for Application as Ultrasensitive Biosensors. *Nano Lett.* **2007**, *7*, 1256–1263.
27. Kabashin, A. V.; Evans, P.; Pastkovsky, S.; Hendren, W.; Wurtz, G. A.; Atkinson, R.; Pollard, R.; Podolskiy, V. A.; Zayats, A. V. Plasmonic Nanorod Metamaterials for Biosensing. *Nat. Mater.* **2009**, *8*, 867–871.
28. Zheng, Y. B.; Yang, Y. W.; Jensen, L.; Fang, L.; Juluri, B. K.; Flood, A. H.; Weiss, P. S.; Stoddart, J. F.; Huang, T. J. Active Molecular Plasmonics: Controlling Plasmon Resonances with Molecular Switches. *Nano Lett.* **2009**, *9*, 819–825.
29. Prodan, E.; Radloff, C.; Halas, N. J.; Nordlander, P. A Hybridization Model for the Plasmon Response of Complex Nanostructures. *Science* **2003**, *302*, 419–422.
30. Hao, F.; Nordlander, P.; Burnett, M. T.; Maier, S. A. Enhanced Tunability and Linewidth Sharpening of Plasmon Resonances in Hybridized Metallic Ring/Disk Nanocavities. *Phys. Rev. B* **2007**, *76*, 245417.
31. Sonnefraud, Y.; Verellen, N.; Sobhani, H.; Vandenbosch, G. A. E.; Moshchalkov, V. V.; Dorpe, P. V.; Nordlander, P.; Maier, S. A. Experimental Realization of Subradiant, Superradiant, and Fano Resonances in Ring/Disk Plasmonic Nanocavities. *ACS Nano* **2010**, *4*, 1664–1670.
32. White, I. M.; Fan, X. On the Performance Quantification of Resonant Refractive Index Sensors. *Opt. Express* **2008**, *16*, 1020–1028.
33. Wu, C. W.; Khanikaev, A. B.; Adato, R.; Arju, N.; Yanik, A. A.; Altug, H.; Shvets, G. Fano-Resonant Asymmetric Metamaterials for Ultrasensitive Spectroscopy and Identification of Molecular Monolayers. *Nat. Mater.* **2012**, *11*, 69–75.
34. Fano, U. Effects of Configuration Interaction on Intensities and Phase Shifts. *Phys. Rev.* **1961**, *124*, 1866–1878.
35. Hao, F.; Larsson, E. M.; Ali, T. A.; Sutherland, D. S.; Nordlander, P. Shedding Light on Dark Plasmons in Gold Nanorings. *Chem. Phys. Lett.* **2008**, *458*, 262–266.
36. Zhang, S.; Genov, D. A.; Wang, Y.; Liu, M.; Zhang, X. Plasmon-Induced Transparency in Metamaterials. *Phys. Rev. Lett.* **2008**, *101*, 047401.
37. Liu, N.; Langguth, L.; Weiss, T.; Kastel, J.; Fleischhauer, M.; Pfau, T.; Giessen, H. Plasmonic Analogue of Electromagnetically Induced Transparency at the Drude Damping Limit. *Nat. Mater.* **2009**, *8*, 758–762.
38. Gallinet, B.; Martin, O. J. F. Relation between Near-Field and Far-Field Properties of Plasmonic Fano Resonances. *Opt. Express* **2011**, *19*, 22167–22175.
39. Yanik, A. A.; Huang, M.; Kamohara, O.; Artar, A.; Geisbert, T. W.; Connor, J. H.; Altug, H. An Optofluidic Nanoplasmonic Biosensor for Direct Detection of Live Viruses from Biological Media. *Nano Lett.* **2010**, *10*, 4962–4969.
40. Chang, T. Y.; Huang, M.; Yanik, A. A.; Tsai, H. Y.; Shi, P.; Aksu, S.; Yanik, M. F.; Altug, H. Large-Scale Plasmonic Microarrays for Label-Free High-Throughput Screening. *Lab Chip* **2011**, *11*, 3596–3602.
41. Palik, E. D. *Handbook of Optical Constants of Solids*; Academic: Orlando, FL, 1985.